Propagation of continental break-up in the southwestern South China Sea

P. HUCHON[1,2], T. N. H. NGUYEN[1] & N. CHAMOT-ROOKE[1]

[1]*Laboratoire de Géologie, Ecole Normale supérieure & CNRS, UMR 8538, 24 rue Lhomond, 75231 Paris Cedex 05, France*

[2]*Present address: Géosciences Azur, Pierre & Marie Curie University & CNRS, UMR 6526, Observatoire océanologique de Villefranche, La Darse, BP 48, 06235 Villefranche-sur-Mer, France (e-mail: huchon@obs-vlfr.fr)*

Abstract: We present new bathymetric, seismic and gravity data on the southwestern tip of the South China Sea oceanic basin, where propagation of continental break-up occurred before *c.* 15 Ma. The oceanic domain has a V-shape typical of oceanic propagating rifts. The tectonic fabric of its margins shows that the main stretching direction was slightly oblique to that of the rift axis. A 2D gravity anomaly inversion, corrected for the thermal effect, is used to estimate the crustal structure. At the continent–ocean boundary, the continental crust is stretched by a factor of about four, rapidly decreasing to about two over a few tens of kilometres, a distance corresponding to just over 1 Ma of break-up propagation. Thus, strain localization occurs at the tip of the propagating oceanic crust just before break-up. The along-axis variation in continental crustal stretching is in good agreement with the kinematics of the oceanic crust derived from magnetic anomalies. This analysis suggests that break-up propagates toward the pole of relative rotation and is primarily controlled by the amount of stretching of the continental crust before oceanization.

Recent studies of continental and oceanic rifts suggest that extension does not occur synchronously along strike. Several models of rift propagation have been proposed (Hey *et al.* 1980; Courtillot 1982; Vink 1982; Bosworth 1985). Hey's concept of oceanic rift propagation differs from models dealing with continental break-up propagation as it implies extension beyond a transform zone of an oceanic rift (spreading centre) into undeformed oceanic lithosphere. In contrast, what we call break-up propagation corresponds to strain localization within a stretched continental lithosphere, i.e. the start of sea-floor spreading. In this regard, the process of strain localization is a direct consequence of the relative motion between two lithospheric plates (Martin 1984). As stretching increases with the distance to the pole of rotation, break-up should initiate away from the pole and propagate towards it, into the stretched continental lithosphere (Vink 1982). Courtillot (1982) presented a different concept of propagation, in which the continental rift is characterized by the presence of 'locked zones' unevenly distributed along the rift axis. Spreading then nucleates between the locked zones, in a way similar to what Bonatti (1985) called punctiform initiation of sea-floor spreading, then propagates into the locked zones. However, McKenzie (1986) pointed out that this mechanism corresponds to strain localization rather than propagation, because the distributed strain in the continental locked zones is progressively replaced by localized strain at the oceanic spreading axis.

In this paper, we attempt to quantify the amount of stretching that occurred during break-up propagation at the tip of the South China Sea basin, one of the best examples of an oceanic basin with a propagating ridge geometry, leading to a typical V-shape. We base our analysis on bathymetry, gravity and seismic data acquired in a 3° × 3° area located at the southwestern tip of the South China Sea (Fig. 1). Through a structural and gravimetric analysis, we estimate the direction and amount of stretching that occurred before break-up, to compare it with the overall kinematics of the opening and to test the various models of propagation.

Kinematic framework

The survey area is located at the southwestern tip of the South China Sea basin (Fig. 1). Early

From: WILSON, R.C.L., WHITMARSH, R.B., TAYLOR, B. & FROITZHEIM, N. 2001. *Non-Volcanic Rifting of Continental Margins: A Comparison of Evidence from Land and Sea.* Geological Society, London, Special Publications, **187**, 31–50. 0305-8719/01/$15.00

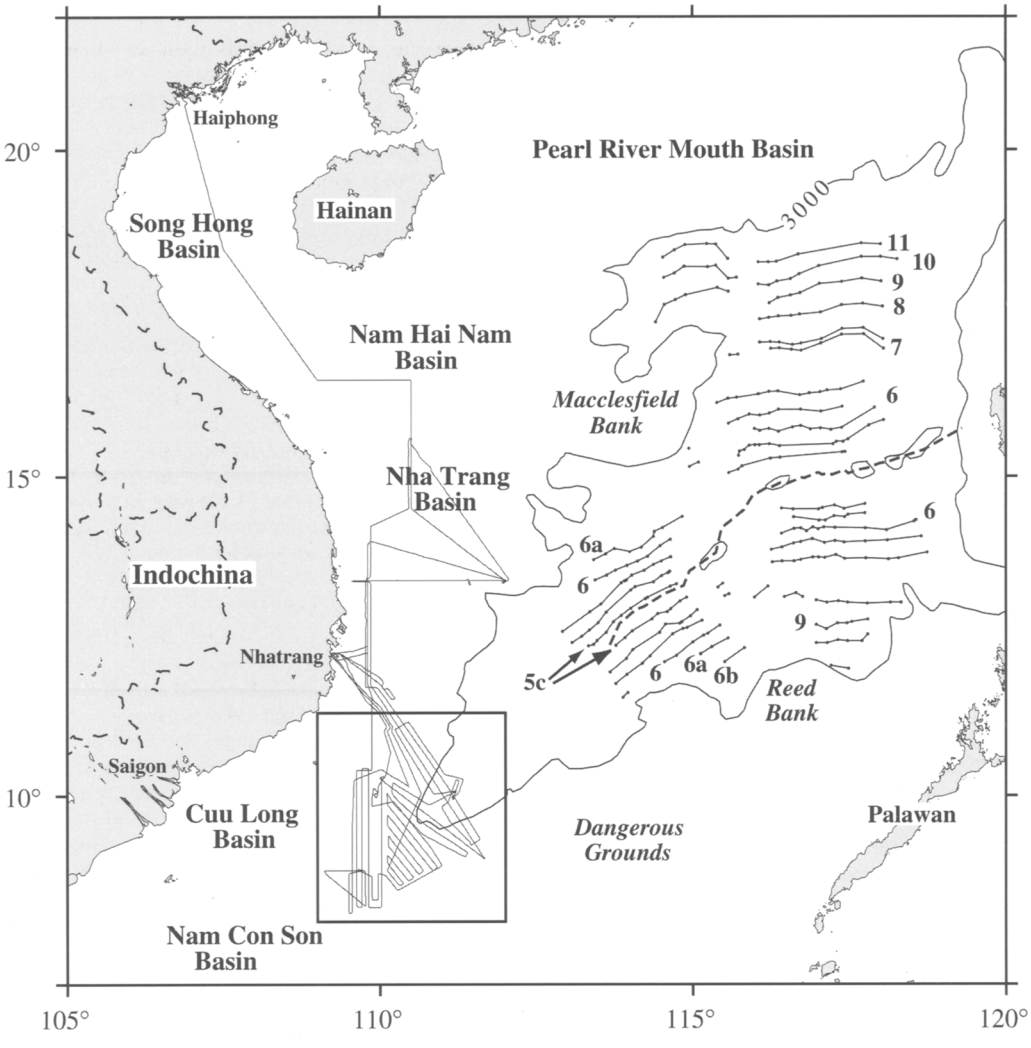

Fig. 1. Location map of the South China Sea. Magnetic anomalies are from Briais *et al.* (1993). Tracks of detailed surveys during the Ponaga cruise are shown. Inset shows location of Figure 2.

work on this basin recognized a typical oceanic basin, based on bathymetry (Chase & Menard 1969), seismic reflection (Emery & Ben-Avraham 1972) and refraction profiles (Ludwig *et al.* 1979), and magnetic profiles (Ben Avraham & Uyeda 1973). The V-shape of the basin mentioned above is well illustrated by the 3000 m isobath (Fig. 1). Taylor & Hayes (1980, 1983) proposed the first comprehensive kinematic model for the opening. They recognized E–W-trending magnetic anomalies 11 to 5D in the eastern part of the basin, corresponding to ages (32–17 Ma, using the time scale of Harland *et al.* (1990)) consistent with the heat flow measurements of Watanabe *et al.* (1977). They also identified the southwestern rift axis with gravity data. This analysis was further extended and refined by Lu *et al.* (1987); Briais *et al.* (1993), who confirmed the age of the onset of spreading at 32 Ma. Furthermore, Briais *et al.* showed that spreading continued until 15 Ma (between anomalies 5B and 5C), after a reorientation of the direction of spreading from N–S to NW–SE shortly after anomaly 7 (23 Ma) (Fig. 1). Pautot *et al.* (1986) and Briais *et al.* (1989) used multibeam bathymetric data to support this reorientation, to which the general trend of the southwestern basin conforms. Magnetic anomalies are not well identified in the southwestern part of the South China Sea. However, the continuity of bathymetric features and the gravimetric signature of the spreading axis

suggests that anomaly 5C should be present at the southwestern tip of the basin.

Although the kinematics of opening of the South China Sea is moderately constrained, the mechanism is much debated. Marginal basins in the western Pacific appear to open (and close) in a large variety of tectonic contexts and have been related either to the effect of subduction (Mariana, Okinawa, Shikoku and Parece Vela Basins) or to the collision of India with Eurasia (Japan Sea, South China Sea) (Jolivet *et al.* (1989) and references therein). The South China Sea is both one of the largest marginal basins and the closest to the collision zone. Analogue experiments (Tapponnier *et al.* 1982) suggest that the basin could have opened at the termination of the left-lateral Red River Fault, as a consequence of the extrusion of the Indochina block. But Taylor & Hayes (1980) suggested that subduction of the proto-South China Sea (south of Reed Bank and Dangerous Grounds) below Palawan and Borneo may have induced its opening by the slab pull effect. These two mechanisms have opposite consequences for the relation between the South China Sea and the Indochina continental margin, which would be a left-lateral strike-slip margin in the extrusion model, whereas the slab pull model predicts a right-lateral margin. Field studies (Rangin *et al.* 1995) have shown that, following a pervasive NW–SE left-lateral strike-slip faulting, the central and southern Vietnam has been affected by large N–S- to N160°E-trending right-lateral strike-slip faulting. To the east of Central Vietnam, analysis of academic and industrial data has led to the conclusion that the N–S-trending margin was active as a dextral transform fault between about 28 and 20 Ma (Marquis *et al.* 1997; Roques *et al.* 1997*a*,*b*). In the basins offshore from southern Vietnam, a kinematic analysis based on crustal structure derived from gravity data led Huchon *et al.* (1998) to recognize dextral decoupling between the opening of the South China Sea and the stretching on the continental margin, also supporting the hypothesis of formation of the South China Sea by southward subduction of the proto-South China Sea.

Geophysical data acquisition and processing

The new data presented here have been acquired during the Ponaga cruise on R.V. *L'Atalante* of 6–30 May 1993 (Fig. 1). They consist of swath bathymetry, six-channel reflection seismic profiles, and 3.5 kHz echo-sounder, gravity and magnetic data. We also dredged at locations where the 3.5 kHz records indicated that basement rocks crop out, mostly on volcanic structures. The Simrad EM 12 dual multibeam bathymetry system enabled us to obtain data in a corridor up to 20 km wide at great depths (>4000 m) and hence to map with full coverage the area shown in Figure 2. The seismic data went through a standard processing sequence: trace editing, common mid-point (CMP) gathering, pulse-shaping and predictive deconvolution, band-pass filtering, stack and f–k (frequency–wavenumber) migration. Processed profiles have been interpreted to produce a structural map, as well as sediment thickness and basement depth maps. The gravity measurements have been corrected for navigational effects and converted to free-air anomalies (Fig. 3). Comparison with the satellite-derived free-air anomaly data (Sandwell & Smith 1992) shows a good agreement, except for the shortest wavelengths (less than 15 km) where the ship data provide more information. The total magnetic field measured using a proton precession magnetometer towed 300 m behind the ship was reduced to magnetic anomalies using the IGRF90 reference field. Comparison of cross tracks, however, showed large discrepancies and we were consequently unable to map the anomalies. As the survey area is located close to the magnetic equator, we tried to apply a correction for the diurnal variation of the magnetic field. Data recorded in the Dalat observatory operated by the Institute of Geophysics of NCNST, Vietnam (11°55'N, 108°25'E) and in a temporary station in Nam Yet island (10°11'N, 114°21'E) show peak-to-peak diurnal variation for quiet days often reaching 150 nT. However, the two sets of data were not consistent and we could not obtain any reliable correction. A plot of the raw data is available in the study by Nguyen (1997).

In the following, we first describe the general structure of the oceanic tip and its margins and then discuss the direction as well as the timing of rifting that will be used as an input for modelling the gravity data in terms of crustal structure.

Shape of the oceanic basin and structure of the margins

The detailed bathymetric map (Fig. 2) shows a typical V-shaped domain whose tip is located near 9°N, 110°E. This domain is limited by a N55°E bathymetric trend to the southeast and a N30°E trend to the northwest. Water depths increase from *c.* 2700 m at the tip to >4000 m

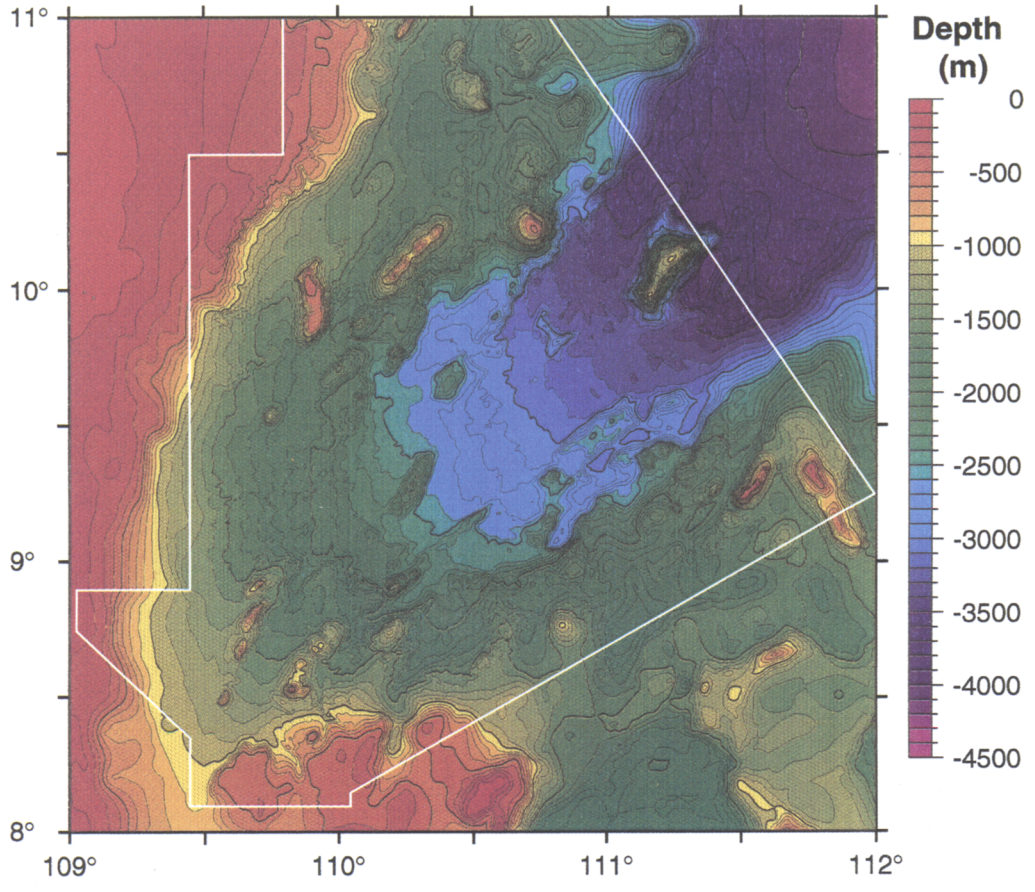

Fig. 2. Detailed bathymetric map (EM12 multibeam data) of the propagating tip of the South China Sea, superimposed on ETOPO5 data. The EM12 survey area is delineated by a white line.

toward the northeast. A large 'butterfly-shaped' volcano occupies the middle of the V-shaped domain near 10°N, 111°15'E. Fresh basalts were dredged from the flank of the volcano, from which a K/Ar age of 4 Ma was obtained (Bellon *et al.* 1994). This volcano, however, is not related to the spreading phase but is part of a large alkalic volcanic event affecting Indochina during Plio-Quaternary time (Flower *et al.* 1996).

Although the area is heavily sedimented, the bathymetry reveals horst and graben structures that parallel the axis of the V-shaped domain, in addition to a few more northerly oriented structures. In Figure 4 we locate the profile Ponaga 9, which shows that the block-faulted margins are clearly separated by an area of highly reflective crust, *c.* 30 km wide (between 90 km and 120 km on the profile, Fig. 5a) and covered by 0.5–1.0 s TWTT (two-way travel time) of post-rift sediment. On the free-air anomaly profile (Fig. 5b), this central area shows low-amplitude peak-to-peak anomalies whereas the stretched continental crust displays higher amplitude, with gravity lows associated with deep basins. We tentatively interpret the deep, central area as underlain by oceanic crust, a hypothesis we shall later test using gravity data modelling. By contrast, the magnetic data show no obvious relationship to the nature of the crust, probably because of the small width of the oceanic domain and the effect of post-spreading volcanism. On the contrary, except over the rift axis, the magnetic anomalies anti-correlate with the free-air anomaly, suggesting normally magnetized continental basement.

The structural map superimposed on the depth to basement (Fig. 6) has been established using the seismic profiles obtained during the cruise (Fig. 4) and complemented by a few industrial profiles. It shows that the deepest basement area (>4500 m) does not strictly

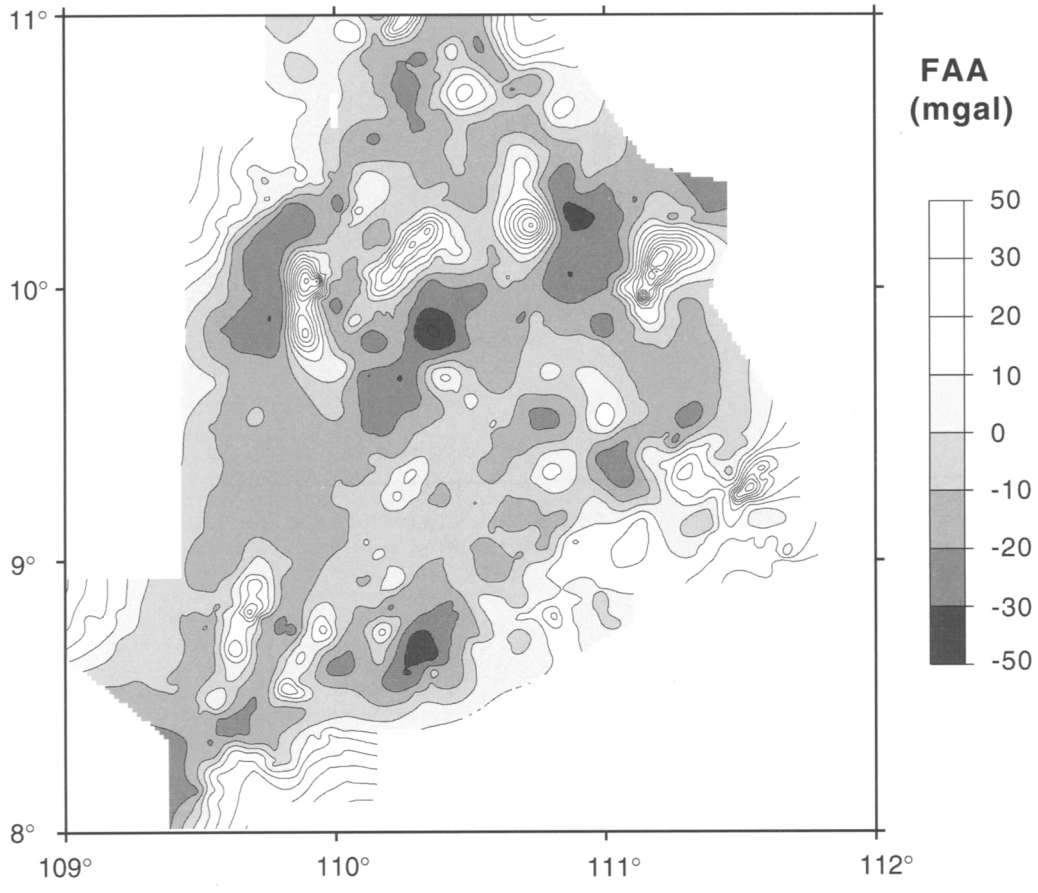

Fig. 3. Free-air gravity anomaly (FAA) map of the propagating tip of the South China Sea.

coincide with the V-shaped domain highlighted by the bathymetry, but also includes a significant part of the lower part of both margins. The northern border of the V-shaped axial domain consists of N30°E–N45°E-trending normal faults, whereas the southern border corresponds to a succession of N45°E–N70°E-trending, right-handed en echelon stepping faults. The tip of the inferred oceanic domain continues into a narrow N45°E-trending depression limited by NW-facing faults, forming a half-graben. At the scale of the whole area, the faulting pattern is dominated by N45°E-trending faults parallel to the axis of the V-shaped domain. This is the main difference between our observations and the scenario devised by Whitmarsh & Miles (1995) for the west Iberia margin, because most of the normal faults on the South China Sea margin do not parallel the continent–ocean boundary, but instead the axis of the oceanic V-shaped domain. However, the fault directions are somewhat scattered, with many N60–70°E-trending faults to the south and more northerly oriented faults (N20–30°E) to the north.

In addition to along-strike variations in the faulting pattern, the structural map (Fig. 6) also reveals an obvious asymmetry. Whereas the southern margin displays mostly NW-facing normal faults, thus facing the rift axis, the northern one shows not only SE-facing faults, but also numerous NW-facing ones, giving rise to an overall asymmetry. This is particularly well expressed at the tip of the V-shaped domain, in the southwest corner of the map, where NW-facing faults delineate a half-graben system. This asymmetry may suggest the occurrence of deep, listric normal faults, which were, however, not imaged on our seismic profiles because of the limited penetration. Listric faults were not imaged on the northern margin of the South China Sea (Pearl River Mouth Basin) by Hayes *et al.* (1995) although they used deep penetration, multi-channel seismic profiles. However, Nissen *et al.* (1995) concluded that

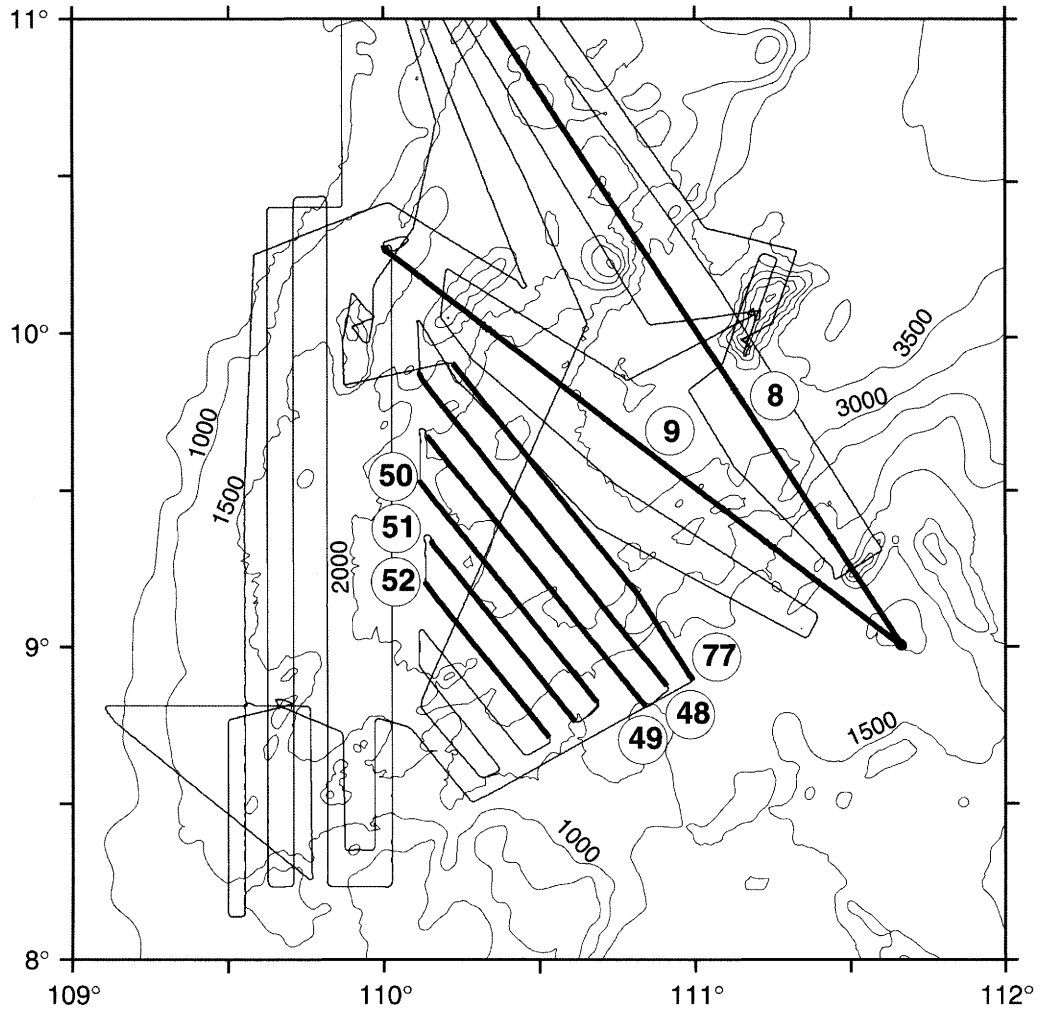

Fig. 4. Location of seismic profiles (bold lines with circled numbers) discussed in the text, superimposed on bathymetry (contour interval 500 m).

matching the observed subsidence and heat flow probably requires a combination of both pure and simple shear in the crust.

Rifting and opening directions

In the studied area, the direction of spreading is not constrained by magnetic anomalies or by transform faults. Hence, it can be only inferred from indirect evidence. In this regard, the N45°E-trending axis of the V-shaped oceanic domain is probably not coincidentally perpendicular to the N136°E direction of motion predicted by Briais *et al.* (1993). This estimate was derived from rotation parameters for the last phase of spreading, from anomaly 5D (17.8 Ma) to the end of spreading at 15.6 Ma. However, the average direction of the normal faults in the stretched continental crust is not strictly parallel to the axis of the propagating oceanic tip, but deviates from the N45°E direction by about 5° (Fig. 7a). In detail, the frequency histogram of Figure 7a shows a slight asymmetry with peaks at N40°E (especially for the area located north of the axis), N50°E and N70°E. This faulting pattern is typical of oblique rifting. Using small-scale models, Tron & Brun (1991) have established experimental histograms of fault directions for various obliquities of rifting. They summarized these experiments in a diagram showing the distribution of the angle between the faults and the rift axis as a function

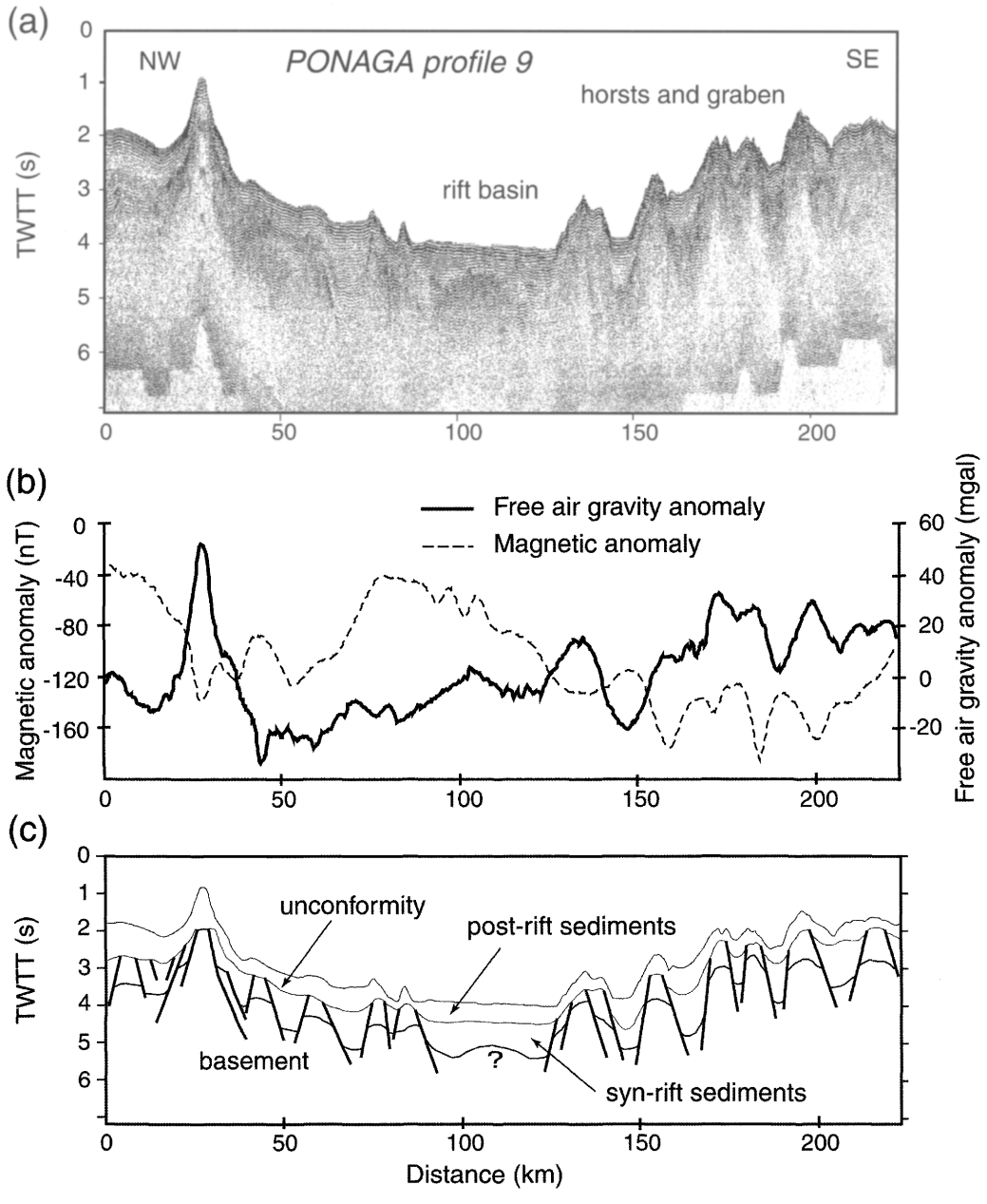

Fig. 5. (**a**) Single-channel seismic profile Ponaga 9 across the propagating tip of the South China Sea. Location indicated in Figure 4. (**b**) Free-air gravity and magnetic anomalies along the same profile. (**c**) Schematic interpretation of the seismic profile. TWTT, two-way travel time.

of the obliquity (Fig. 7b). Comparison of the faulting azimuthal distribution around the tip of the South China Sea (Fig. 7a) with the diagram of Tron & Brun (1991) (Fig. 7b) predicts an obliquity of 25°, and thus a N160°E direction of rifting (Fig. 7c). This is in good agreement with Briais *et al.*'s reconstruction pole for anomaly 6 (20.5 Ma), which predicts a N161°E oriented spreading direction. If one considers that rifting and spreading directions are coaxial, the faulting pattern would then reflect the finite kinematics since 20.5 Ma, and not that of the

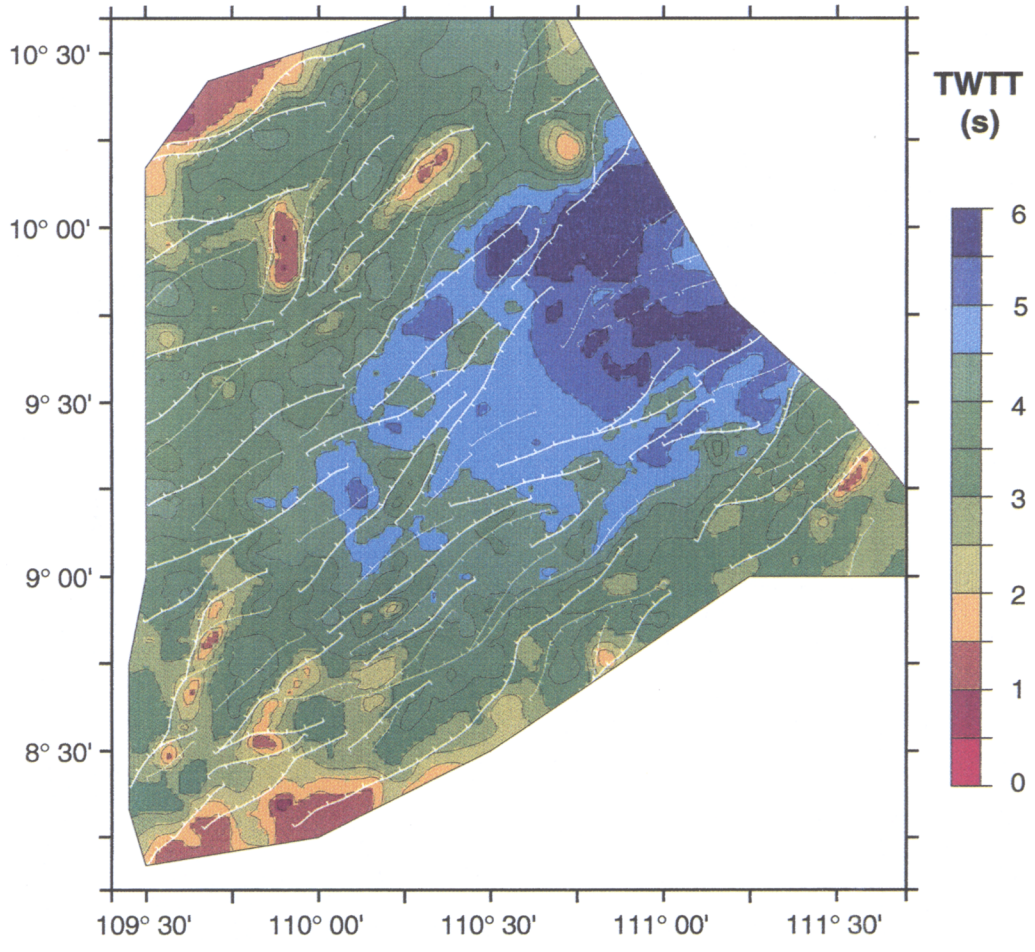

Fig. 6. Structural map of the propagating tip of the South China Sea, superimposed on the depth to basement map (in seconds of two-way travel time; TWTT). Major (>100 m of vertical throw) and minor (<100 m) normal faults are shown by bold and fine fault lines (dashed where unclear), respectively, with ticks on the footwall side.

very last phases of spreading from 17.8 to 15.6 Ma, with a N136°E direction of motion. A N160°E stretching direction implies that the N15°E–N30°E faults (Figs 6 and 7) must have a significant component of dextral strike-slip.

Age of rifting and timing of propagation

The age of the oceanic crust is not constrained in the survey area because the oceanic domain is very narrow and the magnetic anomalies are not well expressed. The magnetic anomaly 5C (16.6 Ma) is the youngest anomaly, identified *c.* 300 km to the NE of the survey area (Fig. 1), and the axis of the extinct oceanic ridge has been estimated to be 15.6 Ma in age (Briais *et al.* 1993). The width of the oceanic crust measured along the N147°E-trending profile Ponaga 8 is *c.* 90 km (Figs 4 and 8). Here, Briais *et al.*'s model predicts a 3.2 cm a^{-1} rate

Fig. 7. (**a**) Cumulated fault length v. azimuth of faults shown in Figure 6. (**b**) Experimental relationship between the obliquity of rifting and the angle between faults and rift axis (redrawn from Tron & Brun 1991). The shaded area is the projection of the fault azimuth histogram: its left and right boundaries are shown by bold lines whereas the two peaks of the histogram are shown by fine lines. The fit of our data to Tron & Brun's diagram is depicted by bold dashed lines. (**c**) Sketch showing the definition of obliquity.

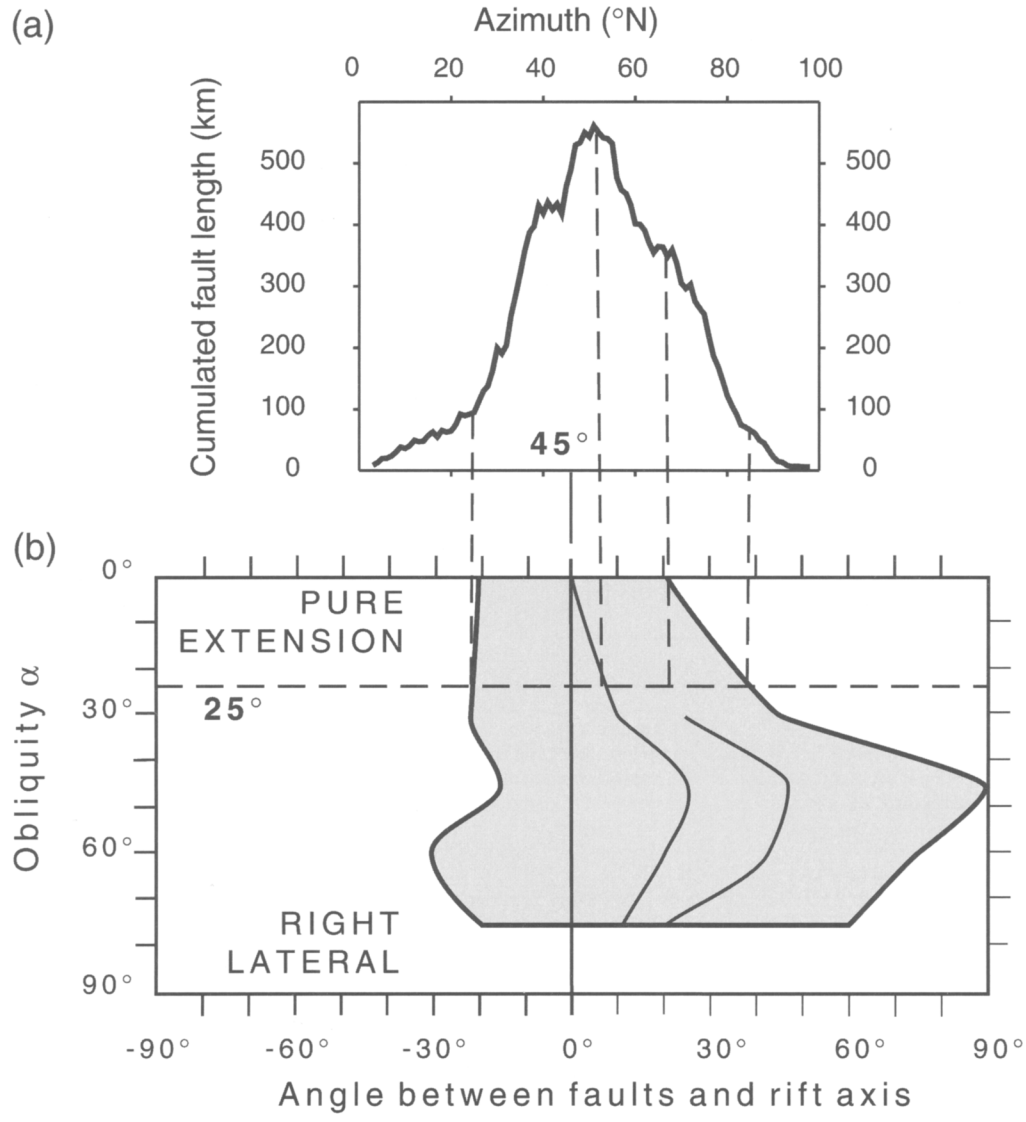
(a)
Azimuth (°N)
0
20
40
60
80
100
Cumulated fault length (km)
500
400
300
200
100
0
45°
(b)
0°
PURE
EXTENSION
25°
30°
60°
RIGHT
LATERAL
90°
Obliquity α
-90°
-60°
-30°
0°
30°
60°
90°
Angle between faults and rift axis

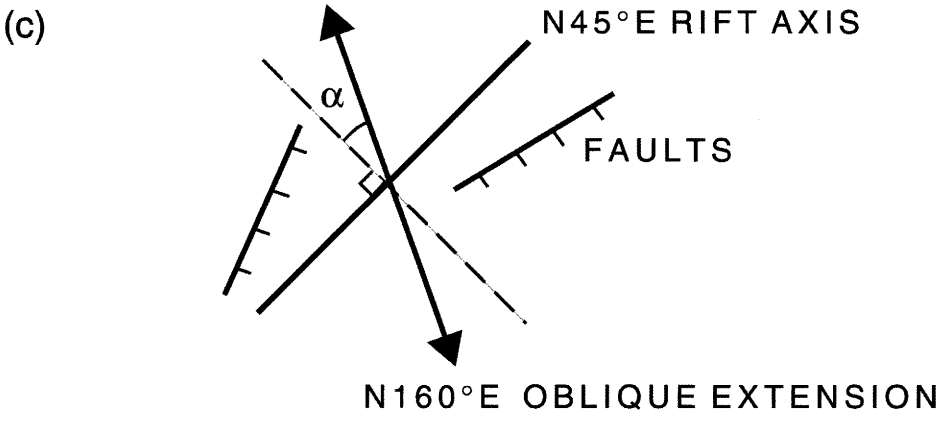
(c)
N45°E RIFT AXIS
α
FAULTS
N160°E OBLIQUE EXTENSION

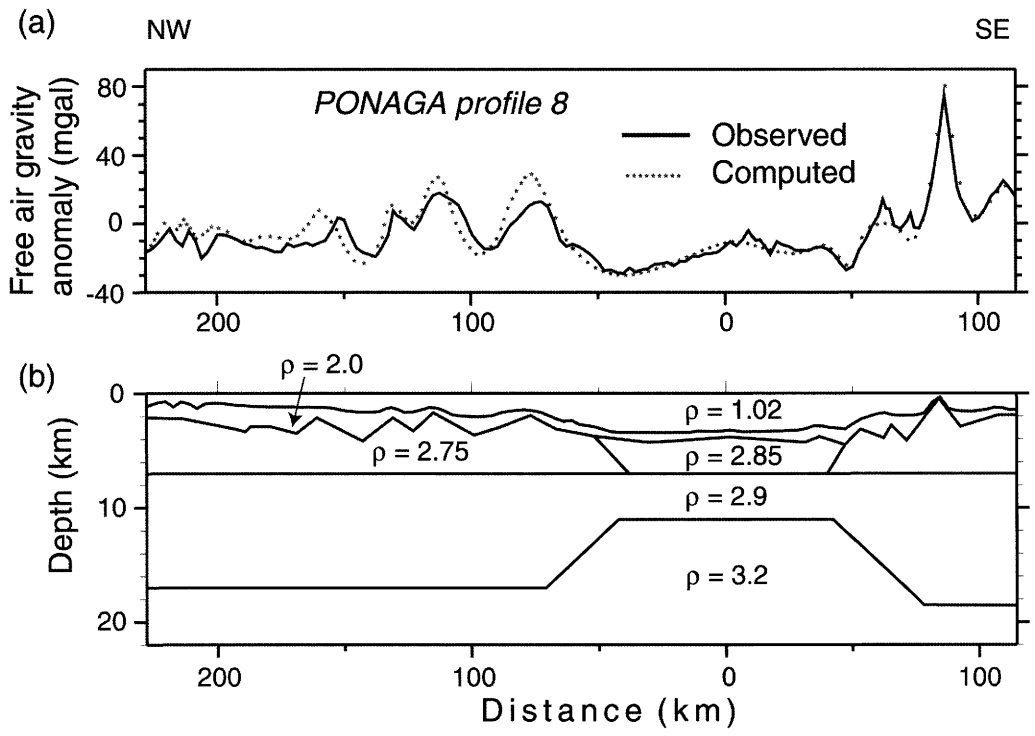

Fig. 8. (**a**) Observed free-air gravity anomaly along profile Ponaga 8 (location indicated in Fig. 4) compared with the anomaly computed using a simple 2D forward modelling technique. (**b**) Geometry and densities (ρ) of layers used for the forward model.

and a N136°E direction of opening during the last phase of spreading, since anomaly 5D (17.8–15.6 Ma). Therefore, the 90 km of oceanic crust seen along profile Ponaga 8 could have been formed in 2.8 Ma, and thus between 18.4 and 15.6 Ma, assuming that spreading ceased at the same time (15.6 Ma) as further to the northeast. This age range is fairly consistent with the depth of the oceanic crust. Unloaded for sediments assuming local isostatic compensation, the average depth of *c.* 4000 m of the oceanic crust corresponds to 18 Ma using the age–depth relationship of Parsons & Sclater (1977). At the scale of the surveyed area, the break-up would thus be diachronous by 3 Ma over a distance of *c.* 100 km. This implies a rate of break-up propagation of *c.* 30 km Ma^{-1}, smaller than the 90 km Ma^{-1} rate computed from the shape of the whole South China Sea (Fig. 1) and the average opening rate since anomaly 7 (*c.* 40 km Ma^{-1}).

The age of the onset of rifting is more difficult to assess. Although rift subsidence in the basins located south of Vietnam is inferred to have started in Late Oligocene time (Matthews *et al.* 1997) or even earlier (during Paleocene–Eocene time) regionally, the major rifting event is marked in the Early Miocene period, with thickening of deposits onto N–S- and NE–SW-oriented normal faults (Matthews *et al.* 1997). Most subsidence curves from industrial wells in the Nam Con Son basin (location shown in Fig. 1) indeed show that subsidence started between 20 and 23 Ma (see, for example, Anonymous 1989). To the north of the survey area, in the Nha Trang Basin (Fig. 1), Marquis *et al.* (1997) suggested that rifting could have started at *c.* 28 Ma, which allows the onset of rifting at the present-day tip of the oceanic crust to be bracketed between 28 and 21 Ma. This would imply a short duration for the rifting phase, between 3 and 10 Ma. Whereas rifting is often considered to have occurred for tens of million years in some basins, it is worth noting that the upper estimate (10 Ma) is that often considered for basins such as the Gulf of Aden (Cochran 1981). Even the 3 Ma lower estimate may not be unreasonable inasmuch as such a short duration of rifting before oceanization has been proved

in the case of the active Woodlark Basin (Taylor *et al.* 1995).

Gravimetric modelling

In the following section, we perform a two-step analysis of the gravity data, to estimate the crustal structure as well as the location of zone of maximum stretching (continent–ocean transition). The first step consists of a simple forward modelling and in the second step we introduce a correction for the thermal structure and perform a 2D inversion of the gravimetric data.

Simple 2D gravity models

We used the values of water depth and sediment thickness (measured on seismic profiles, assuming a 2 km s^{-1} velocity in sediments) to make 2D forward models of the free-air gravity data for profile Ponaga 8, which is nearly perpendicular to the rift axis (Fig. 8). The adopted densities are 1.03 g cm^{-3} for water, 2.85 g cm^{-3} for the upper oceanic crust, 2.75 g cm^{-3} for the upper continental crust, 2.9 g cm^{-3} for the lower crust and 3.2 g cm^{-3} for the mantle. The best-fitting model is consistent with the presence of 7 km thick, probably oceanic crust in the centre of the basin and of thinned continental crust on the edges of the basin. This crude model shows an average thinning factor (in the sense of McKenzie (1978)) of about two over both margins. It also confirms the asymmetry, the continental crust being slightly thinner (by 1.5 km) to the north than to the south.

However, the age of opening of the southwestern tip of the South China Sea is sufficiently recent (*c.* 16 Ma) to still have a significant residual thermal anomaly (e.g. Chamot-Rooke *et al.* 1999). This thermal effect cannot be neglected, because it results in less dense mantle below the rift compared with the flanks, a lateral variation in density that is not taken into account in the simple gravity model.

The 2D inversion of gravity data with thermal correction

The 2D rifting model of Alvarez *et al.* (1984) provides a way to compute the thermal anomaly resulting from the rifting, the spreading and the subsequent cooling phase, taking into account lateral heat conduction and radiogenic heat production in the continental crust. In the studied area, we assumed that the rifting started *c.* 30 Ma ago, which is an upper bound (see discussion above). As discussed above, the estimated 90 km width of oceanic crust corresponds to 2.8 Ma of spreading (from 18.4 to 15.6 Ma). Consequently, the end of rifting, coinciding with the beginning of spreading, was taken at 20 Ma, to account for possible magmatic injection before true oceanic crust emplacement. The end of spreading (beginning of cooling phase) was rounded to 16 Ma. The computed thermal structure for profile Ponaga 8 at 20 Ma, 16 Ma and at the present time is shown in Figure 9. The present-day thermal anomaly results in a gravimetric effect of the order of −100 mgal at the rift axis, decreasing back to nearly zero over a distance of 300 km on both sides.

To perform the inversion of the gravity data, we use the 2D gravity model of Talwani & Ewing (1960), taking the continental crust as the reference layer with a density $\rho_c = 2.75$ g cm^{-3}. The mantle Bouguer anomaly g_b is then the sum of the observed free-air anomaly g_{obs} and the gravimetric contributions of the various layers: the anomaly g_w due to water of density $\rho_w = 1.03$ g cm^{-3}; the anomaly g_s due to sediments of average density $\rho_s = 2.0$ g cm^{-3}; the anomaly g_{co} due to the presence of oceanic crust with a density $\rho_{co} = 2.85$ g cm^{-3}, instead of continental crust (the boundary of which is adjusted iteratively to fit the observed anomaly); the anomaly g_T caused by the thermal anomaly T with a density $\rho_m = \rho_{mo}(1 - \alpha T)$, where $\rho_{mo} = 3.3$ g cm^{-3} and α is the thermal expansion coefficient.

To compute the gravimetric Moho, we used a 2D inversion by fast Fourier transform (FFT). The gravity effect of the Moho interface with variation $h(x)$, density contrast $\Delta\rho_m = \rho_m - \rho_c$ at a mean depth d, provided that $d \gg h(x)$ (Parker 1972) can be approximated by

$$g(x) = 2\pi\Delta\rho G h(x) e^{-kd}$$

where G is the universal constant of gravitation and k is the wavenumber. In the Fourier domain we can write

$$G(k) = 2\pi\Delta\rho G H(k) e^{-kd}$$

Here, $G(k) = TF[g(x)]$ and $H(k) = TF[h(x)]$, where TF is the direct Fourier transform. Hence, we can determine undulations $h(x)$ of the gravimetric Moho by the inverse Fourier transform (TF^{-1}) of $H(k)$:

$$h(x) = TF^{-1}[H(k)] = TF^{-1}\left[\frac{G(k)}{2\pi G\Delta\rho e^{-kd}}\right]$$

$$= TF^{-1}\frac{TF[g(x)]}{2\pi G\Delta\rho e^{-kd}}$$

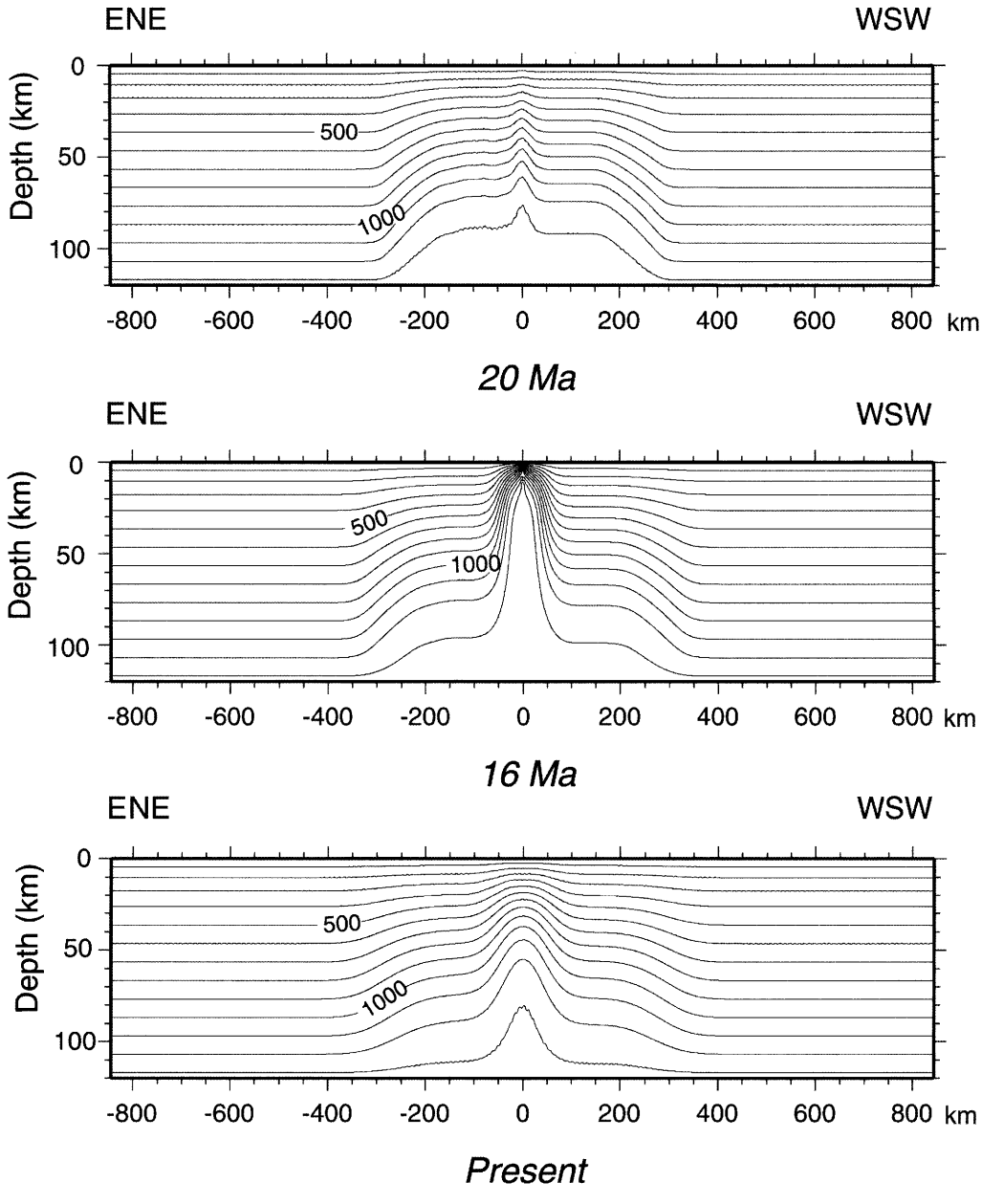

Fig. 9. Isotherms (in °C) computed for profile Ponaga 8 using the 2D rifting model of Alvarez *et al.* (1984), shown at 20 Ma (beginning of spreading), 16 Ma (end of spreading) and at present.

Figure 10 shows the result of the inversion for the profile Ponaga 8. The calculated thickness of what we interpret as oceanic crust is *c.* 6 km, whereas that of the continental crust varies between 8 km near the continent–ocean boundary and 20 km at 150 km to the northwest. The shape of the Moho is obviously more realistic than with the simple forward modelling, which provided only an estimate of the mean Moho depth. For comparison, we also computed the depth to the isostatic Moho, which is obtained by summing the water depth h_w, the sediment

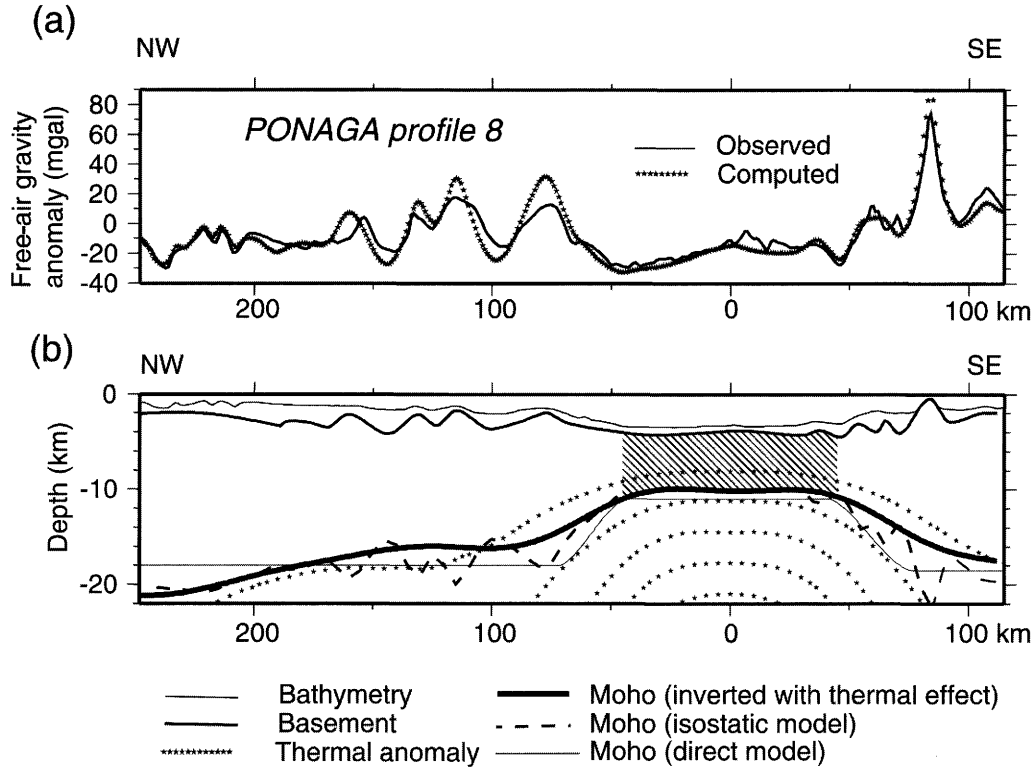

Fig. 10. (**a**) Observed free-air gravity anomaly along profile Ponaga 8 compared with the anomaly computed from the model shown in (**b**) with the Moho derived from the 2D inversion of gravity data, including the thermal effects of rifting and spreading as discussed in the text. (**b**) Comparison of the depth to Moho inverted with thermal effect with the depth obtained by forward modeling as in Fig. 8 and by a local isotatic model. The bathymetry to top of basement and the thermal anomaly (contoured interval 50°C) derived from Figure 9 are also shown.

thickness h_s and the crustal thickness h_c obtained by isostatically unloading the sediments:

$$h_c = H - [h_w(\rho_c - \rho_w) + h_s(\rho_c - \rho_s)]/(\rho_m - \rho_c)$$

In this equation, H is the initial crustal thickness (before stretching), taken as 30 km to be consistent with the observed crustal thickness along the coast of Vietnam (Bui 1993). The Moho obtained by inversion is smoother than the isostatic Moho because of the filtering by FFT, but also slightly higher as it takes into account the lateral variation of density.

The crustal structures obtained for the eight profiles identified in Figure 4 have several common features (Fig. 11): (1) a 6–7 km thick oceanic crust in the centre of the basin (profiles 8, 9, 77 and 48), which narrows towards the southwest (90 km on profile 8, 30 km on profile 48); (2) a narrow (*c.* 10 km) transition zone between oceanic crust and continental crust; (3) a thinned continental crust on the basin edges, with Moho depths ranging from 17 to 21 km in the north and slightly deeper on the southern margin; this confirms that the continental crust is asymmetrically thinned.

In the following sections, we first explore the consequences of these results in terms of the geometry of the ocean–continent boundary and the nature of continental crustal extension before break-up. We then use these data to derive the kinematics of rifting.

Continent–ocean boundary and continental crust stretching

A primary result of the gravimetric modelling is the crustal thickness map shown in Figure 12. Outside of the area where the crustal thickness is constrained by our gravity modelling, we used the regional crustal thickness map of Huchon *et al.* (1998), obtained from a 3D inversion of

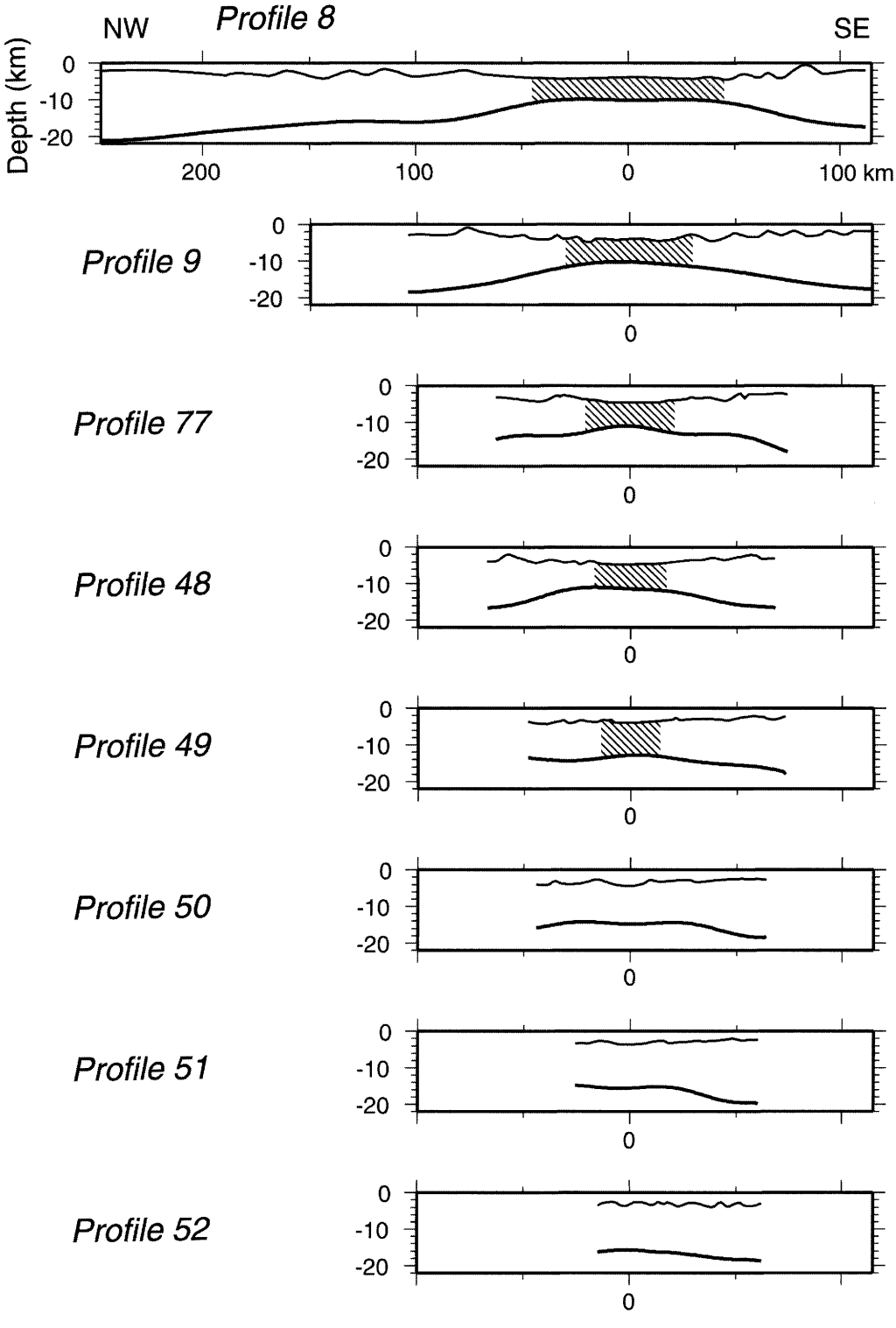
NW
Profile 8
SE
Depth (km)
0
-10
-20
200
100
0
100 km
Profile 9
Profile 77
Profile 48
Profile 49
Profile 50
Profile 51
Profile 52

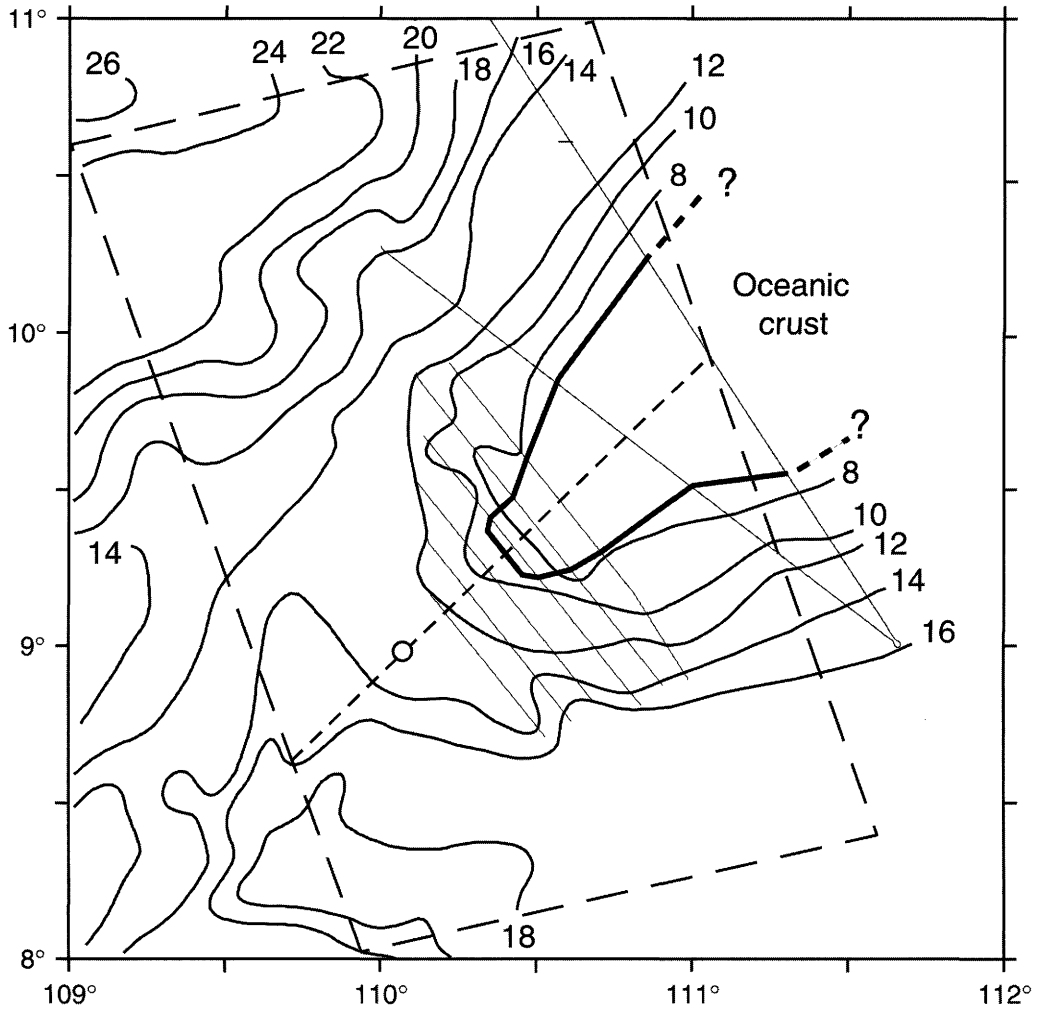

Fig. 12. Continental crustal thickness map (in km) obtained using the eight profiles of Figure 10 (shown by fine lines) complemented with a regional estimate of the crustal thickness (Huchon *et al.* 1998). Bold line: continent–ocean boundary; short-dashed line, *x*-axis of Figures 12 and 13; long-dashed line delineates the area of computation for Figure 14.

gravity data over the South Vietnam shelf, without correction for thermal effect. In areas where the two datasets overlap, the agreement is fair, with <2 km offsets. On the same map, we also plot the location of the continent–ocean boundary obtained from the gravity modelling. The corresponding width of the oceanic crust is plotted in Figure 13a. Figure 13b shows the crustal thickness measured along the axis of the oceanic propagating crust (shown as a short-dashed line in Fig. 12). Whereas on profiles 8, 9, 77 and 48 the crustal thickness is nearly constant and typical of oceanic crust (6.5–7 km), it rapidly increases toward the southwest on profiles 49, 50, 51 and 52 (Fig. 13b). The nature of the crust on profile 49, where the crustal thickness is *c.* 9 km, is questionable. The gravity data on this profile are best modelled with a denser

Fig. 11. Crustal structure obtained by 2D inversion of gravity data along eight profiles across the propagating tip of the South China Sea (location shown in Fig. 4). Shaded area is inferred oceanic crust.

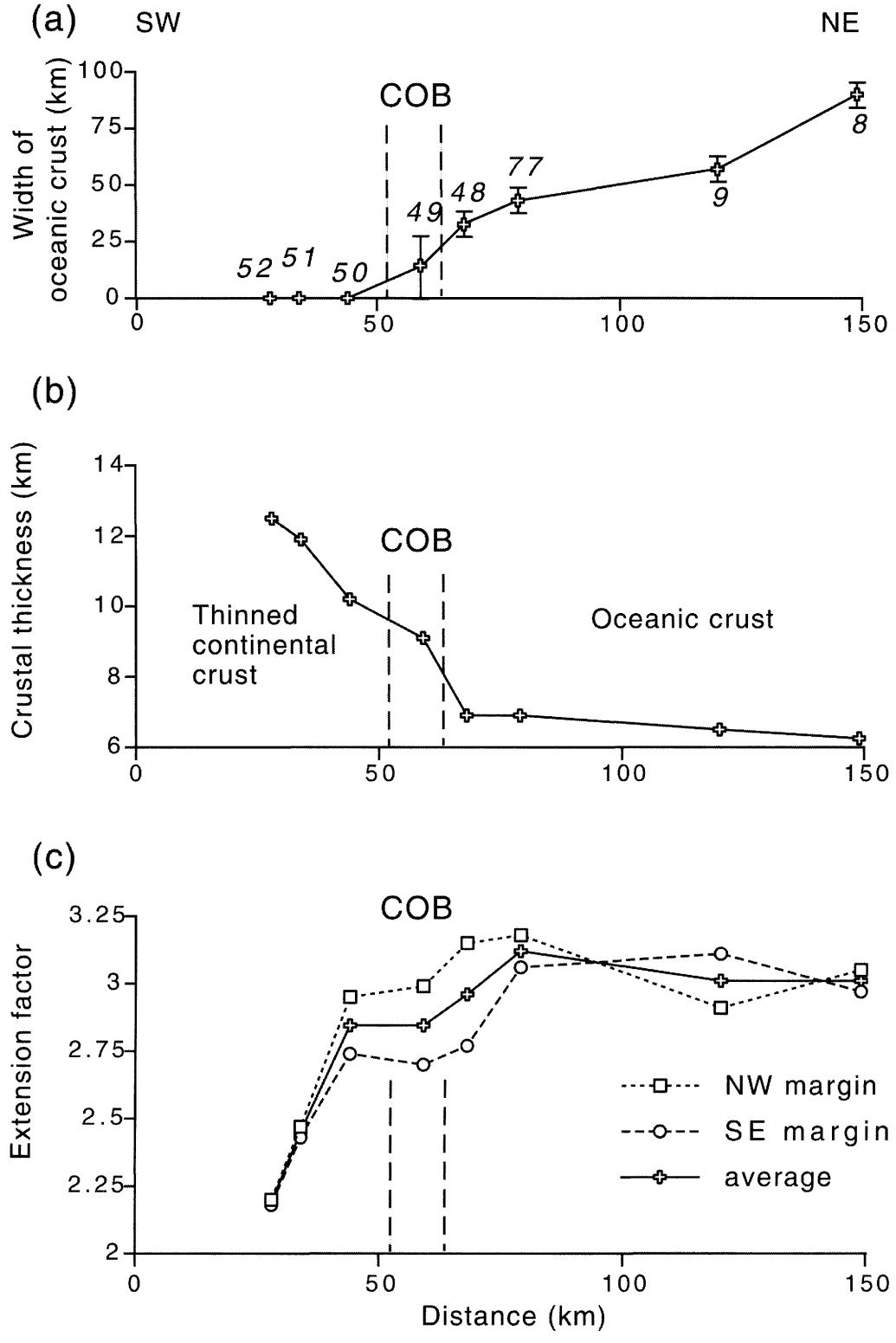
(a)
SW
NE
Width of oceanic crust (km)
100
75
50
25
0
COB
52
51
50
49
48
77
9
8
0
50
100
150
(b)
Crustal thickness (km)
14
12
10
8
6
COB
Thinned continental crust
Oceanic crust
0
50
100
150
(c)
Extension factor
3.25
3
2.75
2.5
2.25
2
COB
NW margin
SE margin
average
0
50
100
150
Distance (km)

upper crust in the middle part of the profile (see Fig. 11), suggesting the presence of oceanic crust.

However, there is an obvious trade-off between the shape of the Moho and the density of the crustal layer, so that gravity alone cannot solve simultaneously for Moho shape and width of the oceanic crust. Based on the thermal models of generation of the oceanic crust, we see no rational way to increase the oceanic crust thickness at the tip of the propagator, at least in a permanent regime of propagation. Larger oceanic crust thickness at the propagator tip may thus be a transient effect related to the dying rift. The obvious alternative is that the crust is continental on profile 9. We conclude that the total width of the oceanic crust on this profile is between 0 and 25 km (Fig. 13a).

The similarity between the highly thinned area ahead of the tip of the propagating oceanic rift and the outer continental margin on both sides of the V-shaped domain is illustrated in Figure 13c. The mean stretching factor in a strip 50 km wide, running parallel to the inferred continent–ocean boundary on both sides of the oceanic crust is about three. It slightly decreases on profiles 49 and 50 to a value of 2.85 then suddenly decreases to 2.5 (profile 51) and 2.2 (profile 52). This suggests that oceanic propagation occurs when the continental crust in front of the propagating tip is stretched enough (<10 km) to allow oceanic spreading to start. On the various profiles analysed, the crustal thickness at the continent–ocean boundary ranges from 7 to 10 km. The corresponding threshold stretching factor of three to four for break-up is that generally considered for mechanical reasons (see, for example, Le Pichon & Sibuet 1981).

In more detail, the crustal thickness mapped in Figure 12 and the stretching factors plotted in Figure 13c reveal the asymmetry of rifting already pointed out. Although the situation is reversed on profile 9, the average stretching factor within 50 km of the continent–ocean boundary is larger to the northwest, compared with the southeast (Fig. 13c), an observation consistent with both the depth to basement map (Fig. 6) and the free-air gravity anomaly map (Fig. 3), which shows that basins are deeper to the northern side of the propagating tip compared with the southern side. This can be explained by the obliquity of rifting, as the direction of propagation (toward azimuth N225°E) is directed more southeastward than the mean trend of normal faults (N50°E, or N230°E), leaving more extended crust to the northwest.

Break-up propagation and oceanic kinematics

In the model we envision the propagation of sea-floor spreading follows the model of Martin (1984), in which the sum of oceanic spreading and continental stretching should coincide with the amount of separation between the plates, and thus be described by the rules of plate kinematics. Taken in the simplest way, extension should decrease towards the pole of rotation. To test this idea, and thus to compare the amount of extension corresponding to the crustal thickness map of Figure 12 with the prediction of oceanic kinematics, we measured the continental crustal thickness along N160°E-trending sections on the map of Figure 12. We then converted the crustal thickness profiles into horizontal stretching, assuming an initial 30 km thick continental crust, equal to the present-day crustal thickness in the unstretched coastal area of South Vietnam (Bui 1993). These are, of course, lower estimates, as they ignore the stretching that occurred on the inner (or upper part) of the margin, to the north and to the south of the studied area. However, the stretching factor in this area is small (*c.* 1.2) and, given an approximate width of 150 km, would result in an additional 30 km of stretching at most, compared with *c.* 130 km for the outer (or lower) part of the margin (Fig. 14). We also measured the width of the oceanic crust along the same profiles. Whereas the amount of sea-floor spreading decreases toward the southwest, the amount of continental stretching slightly increases (Fig. 14). This is only an apparent paradox because the continental crust located ahead of the propagating oceanic crust could be subjected to stretching for a longer period of

Fig. 13. (**a**) Width of the oceanic crust measured along the eight profiles where gravity data have been modelled (location shown in Fig. 4) and plotted along the axis of the propagating tip of the South China Sea (location shown in Fig. 12). The origin is taken at the tip of the V-shaped domain (9°N, 110°E). COB, continent–ocean boundary. The larger error bar for profile 49 should be noted (see discussion in text). (**b**) Along-axis variation in crustal thickness; *x*-axis as in (**a**). (**c**) Extension factor of the continental crust measured in a 50 km wide strip parallel to the continent–ocean boundary; *x*-axis as in (**a**). The northwestern and southeastern margins are plotted separately to show the asymmetry.

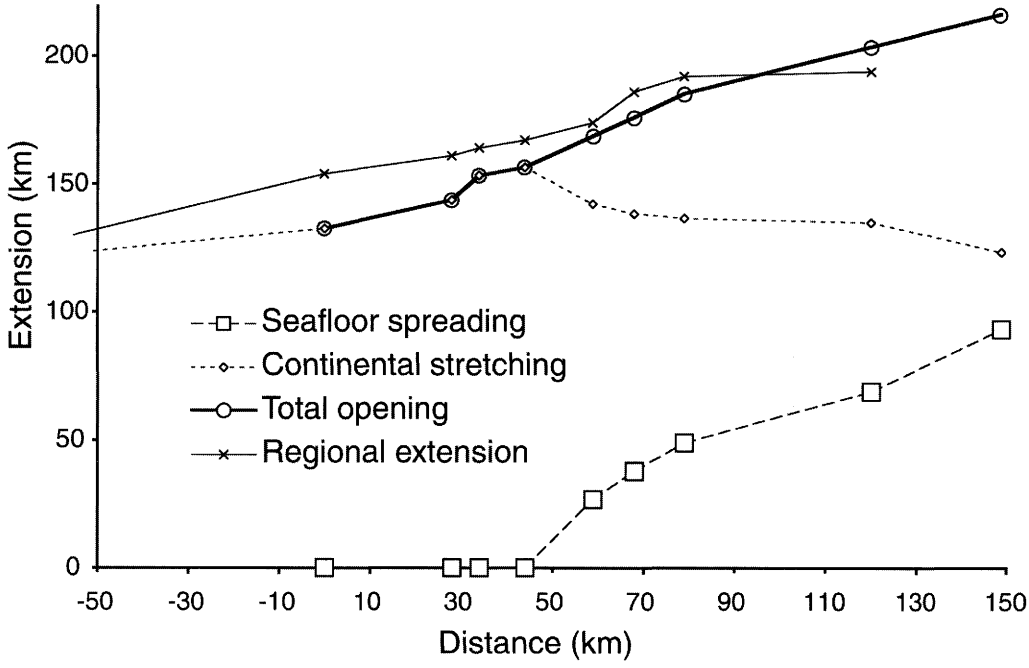

Fig. 14. Variation in the amount of oceanic spreading and continental stretching along the axis of the propagating tip of the South China Sea. Origin and *x*-axis as in Figure 13 (see Fig. 12 for location). The values have been computed along N160°E-trending, 300 km long profiles in the dashed box shown in Figure 12. The total opening (spreading plus stretching) shows a decrease toward the southwest that predicts a pole of rotation located *c.* 285 km to the southwest (see text). The regional extension computed by Huchon *et al.* (1998) is shown for comparison.

time than that on both sides of the oceanic crust. In our case, the amount of oceanic spreading decreases southwestward from 90 km to zero whereas the amount of continental stretching increases from 125 km to 155 km. The sum is then decreasing toward the southwest (Fig. 14). It is noteworthy that the same observation of increasing continental extension toward the pole of relative rotation has been made in the Woodlark Basin (see Taylor *et al.* 1999, fig. 5).

For comparison, we also show in Figure 14 the amount of extension estimated by Huchon *et al.* (1998) from a 3D gravity model of the South Vietnam basins. The agreement is fair, except to the northeast where our estimate is larger: this is because Huchon *et al.* did not take into account the amount of oceanic spreading, leading to an underestimation of the extension to the northeast. The profiles used by Huchon *et al.* were slightly longer (350 km instead of 300 km here); however, the difference is only about 10 km, showing that the stretching of the inner margin is almost negligible with respect to that of the most stretched area around the oceanic propagating tip.

The least-squares fit of the total opening curve in Figure 14 shows that the corresponding pole of rotation must be located 285 km to the southwest of the oceanic tip (taken at profile 49), not far from the pole of finite rotation for anomaly 5D (5°N, 105.5°E) of Briais *et al.* (1993). Again, we should stress that we do not take into account the stretching of the inner margin, outside the surveyed area. This would result in a slightly more distant pole of rotation, which incidentally would better fit with the pole of finite rotation determined from magnetic anomalies. Such an agreement between two totally independent data sets therefore suggests that the Martin (1984) model of strain localization can be considered as basically valid in the case of the South China Sea.

Conclusion

In spite of a complex geodynamic setting, the propagation of break-up in the southwestern South China Sea appears to have occurred in a rather simple way, with spreading occurring as soon as thinning of the continental crust reaches a factor of about four. Ahead of the propagating

tip, the stretching factor drops from this value to a value of two over a distance of *c.* 40 km. The continental crust thus thins from *c.* 15 km to <10 km over a distance corresponding to just over 1 Ma of break-up propagation. Compared with the average thinning during the total rifting period, with an estimated duration of 3–10 Ma, this observation suggests that strain localization, as expected, does occur at the tip of the propagating oceanic crust just before break-up. This has been best demonstrated in the case of the active Woodlark Basin, where the local strain rate immediately preceding break-up is often one or two orders of magnitude larger than the average strain rate across the whole margin (Taylor *et al.* 1999).

We warmly thank the captain, officers and crew of the R.V. *L'Atalante*, as well as the GENAVIR technical team. IFREMER and CNRS–INSU supported the cost for operations and travel, respectively. Additional funding for data processing was provided by CNRS–INSU through a 'Géosciences marines' grant. Nguyen Thi Kim Thoa kindly provided us with magnetic data from Vietnamese observatories. Maps were prepared using the GMT freeware (Wessel & Smith 1991). The paper benefited from the careful reviews of R. Hey, B. Taylor and an anonymous referee. This paper is UMR Géosciences Azur Contribution 336.

References

ALVAREZ, F., VIRIEUX, J. & LE PICHON, X. 1984. Thermal consequences of lithosphere extension over continental margins: the initial stretching phase. *Geophysical Journal of the Royal Astronomical Society*, **78**, 389–411.

Anonymous *Report on Comprehensive Investigation and Research of Nansha Islands and Adjacent Maritime Regions*. Academia Sinica Publishing House, Beijing.

BELLON, H., RANGIN, C. & HUCHON, P. 1994. Late Miocene to Quaternary volcanism of Vietnam: time and space geochemical variations (abstract). *Cenozoic Evolution of the Indochina Peninsula, Hanoi and Do Son, Vietnam, 25–29 April 1994*, 47–48.

BEN AVRAHAM, Z.B. & UYEDA, S. 1973. The evolution of the China basin and the Mesozoic paleogeography of Borneo. *Earth and Planetary Science Letters*, **18**, 365–376.

BONATTI, E. 1985. Punctioform initiation of seafloor spreading in the Red Sea during transition from a continental to an oceanic rift. *Nature*, **316**, 33–37.

BOSWORTH, W. 1985. Geometry of propagating continental rifts. *Nature*, **316**, 625–627.

BRIAIS, A., PATRIAT, P. & TAPPONNIER, P. 1993. Updated interpretation of magnetic anomalies and reconstructions of the South China basin: implications for the Tertiary evolution of Southeast Asia. *Journal of Geophysical Research*, **98**, 6299–6328.

BRIAIS, A., TAPPONNIER, P. & PAUTOT, G. 1989. Constraints of SeaBeam data on crustal fabrics and seafloor spreading in the South China Sea. *Earth and Planetary Science Letters*, **95**, 307–320.

BUI, C.Q. 1993. Some characteristics of the deep crustal structure and the geodynamics in the territory of Viet Nam and neighbouring sea area. *Journal of Geology, Geological Society of Vietnam*, **1-2**, 39–50.

CHAMOT-ROOKE, N., GAULIER, J.M. & JESTIN, F. 1999. Constraints on Moho depth and crustal thickness in the Liguro-Provençal Basin from a 3D gravity inversion: geodynamic implications. *In*: DURAND, B., JOLIVET, L., HORVÁTH, F. & SÉRANNE, M. (eds) *The Mediterranean Basins: Tertiary Extension within the Alpine Orogen*. Geological Society, London, Special Publications, **156**, 37–61.

CHASE, T.E. & MENARD, H.W. *Bathymetric Atlas of the Northwestern Pacific*. US Naval Oceanographic Office, Washington, DC.

COCHRAN, J.R. 1981. The Gulf of Aden: structure and evolution of a young ocean basin and continental margin. *Journal of Geophysical Research*, **86**, 263–287.

COURTILLOT, V. 1982. Propagating rifts and continental breakup. *Tectonics*, **1**, 239–250.

EMERY, K.O. & BEN-AVRAHAM, Z. 1972. Structure and stratigraphy of China Basin. *AAPG Bulletin*, 5, **56**, 839–859.

FLOWER, M., NGUYEN, H., NGUYEN, X.B. & NGUYEN, T.Y. 1996. Implications for basalt major element compositions for melting beneath Indochina: response to reorganised spreading and thermally-anomalous asthenosphere. *Bulletin de la Société Géologique de France*, 6, **167**, 773–784.

HARLAND, W.B., ARMSTRONG, R.L., COX, A.V., CRAIG, L.E. & SMITH, A.G. *A Geologic Time Scale 1989*. Cambridge University Press, Cambridge.

HAYES, D.E., NISSEN, S.S., BUHL, P. & DIEBOLD, J. 1995. Throughgoing crustal faults along the northern margin of the South China Sea and their role in crustal extension. *Journal of Geophysical Research*, **100**, 22435–22446.

HEY, R.N., DUENNEBIER, F.K. & MORGAN, W.J. 1980. Propagating rifts on mid-ocean ridges. *Journal of Geophysical Research*, **85**, 3647–3658.

HUCHON, P., NGUYEN, T.N.H. & CHAMOT-ROOKE, N. 1998. Finite extension across the South Vietnam basins from 3D gravimetric modeling: relation to South China Sea kinematics. *Marine and Petroleum Geology*, **15**, 619–634.

JOLIVET, L., HUCHON, P. & RANGIN, C. 1989. Tectonic setting of western Pacific marginal basins. *Tectonophysics*, **160**, 23–47.

LE PICHON, X. & SIBUET, S. 1981. Passive margins: a model of formation. *Journal of Geophysical Research*, B5, **86**, 3708–3720.

LU, W., KE, C., WU, J., LIU, J. & LIN, C. 1987. Characteristics of magnetic lineations and tectonic evolution of the South China Sea basin. *Acta Oceanologica Sinica*, **6**, 577–588.

LUDWIG, W.J., KUMAR, N. & HOUTZ, R.E. 1979. Profiler-Sonobuoy measurements in the South China Sea basin. *Journal of Geophysical Research*, **84**, 3505–3518.

MARQUIS, G., ROQUES, D., HUCHON, P., COULON, O., CHAMOT-ROOKE, N., RANGIN, C. & LE PICHON, X. 1997. Amount and timing of extension along the continental margin off central Vietnam. *Bulletin de la Société Géologique de France*, 6, **168**, 15–24.

MARTIN, A.K. 1984. Propagating rifts: crustal extension during continental rifting. *Tectonics*, **3**, 611–617.

MATTHEWS, S.J., FRASER, A.J., LOWE, S., TODD, S.P. & PEEL, F.J. 1997. Structure, stratigraphy and petroleum geology of the south east Nam Con Son basin, offshore Vietnam. *In*: FRASER, A.J., MATTHEWS, S.J. & MURPHY, R.W. (eds) *Petroleum Geology of South East Asia*. Geological Society, London, Special Publications, **126**, 89–106.

MCKENZIE, D.P. 1978. Some remarks on the development of sedimentary basins. *Earth and Planetary Science Letters*, **40**, 25–32.

MCKENZIE, D.P. 1986. The geometry of propagating rifts. *Earth and Planetary Science Letters*, **77**, 176–186.

NISSEN, S.S., HAYES, D.E., YAO, B., ZENG, W., CHEN, Y. & NU, X. 1995. Gravity, heat flow, and seismic constraints on the process of crustal extension: northern margin of the South China Sea. *Journal of Geophysical Research*, **100**, 22447–22483.

NGUYEN, T.N.H. 1997. Structure et cinématique de l'extrémité de la Mer de l'Est (Mer de Chine méridionale) et des bassins du sud Vietnam. PhD thesis, University of Paris 6.

PARKER, R.L. 1972. The rapid computation of potential anomalies. *Geophysical Journal of the Royal Astronomical Society*, **31**, 447–455.

PARSONS, B. & SCLATER, J.G. 1977. An analysis of the variation of ocean floor bathymetry and heat flow with age. *Journal of Geophysical Research*, **82**, 803–827.

PAUTOT, G., RANGIN, C., BRIAIS, A. & 9 OTHERS 1986. Spreading direction in the central South China Sea. *Nature*, **321**, 150–154..

RANGIN, C., HUCHON, P., BELLON, H., NGUYEN, D.H., LE PICHON, X., PHAN, V.Q. & ROQUES, D. 1995. Cenozoic deformation of central and south Vietnam: evidences for superposed tectonic regimes. *Tectonophysics*, 1-4, **251**, 179–196.

ROQUES, D., MATTHEWS, S.J. & RANGIN, C. 1997*a*. Constraints on strike-slip motion from seismic and gravity data along the Vietnam margin offshore Danang: implications for hydrocarbon prospectivity and opening of the East Vietnam Sea. *In*: FRASER, A.J., MATTHEWS, S.J. & MURPHY, R.W. (eds) *Petroleum Geology of South East Asia*. Geological Society, London, Special Publications, **126**, 342–353.

ROQUES, D., RANGIN, C. & HUCHON, P. 1997*b*. Geometry and sense of motion along the Vietnam continental margin: onshore/offshore Da Nang area. *Bulletin de la Société Géologique de France*, 4, **168**, 413–422.

SANDWELL, D.T. & SMITH, W.H.F. 1992. Global marine gravity from ERS-1, Geosat and Seasat reveals new tectonic fabric. *EOS Transactions, American Geophysical Union*, 43, **73**, 133.

TALWANI, M. & EWING, M. 1960. Rapid computation of gravitational attraction of three-dimensional bodies of arbitrary shape. *Geophysics*, 1, **25**, 203–225.

TAPPONNIER, P., PELTZER, G., LE DAIN, A.Y., ARMIJO, R. & COBBOLD, P. 1982. Propagating extrusion tectonics in Asia: new insights from simple experiments with plasticine. *Geology*, **10**, 611–616.

TAYLOR, B. & HAYES, D.E. 1980. The tectonic evolution of the South China basin. *In*: HAYES, D.E. (ed.) *The Tectonic and Geologic Evolution of Southern Asian Seas and Islands. Part 1*. Geophysical Monographs, American Geophysical Union, **23**, 89–104.

TAYLOR, B. & HAYES, D.E. 1983. Origin and history of the South China Basin. *In*: HAYES, D.E. (ed.) *The Tectonic and Geologic Evolution of Southern Asian Seas and Islands. Part 2*. Geophysical Monographs, American Geophysical Union, **27**, 23–56.

TAYLOR, B., GOODLIFFE, A. & MARTINEZ, F. 1999. How continents break up: insights from Papua New Guinea. *Journal of Geophysical Research*, **104**, 7497–7512.

TAYLOR, B., GOODLIFFE, A., MARTINEZ, F. & HEY, R. 1995. Continental rifting and initial sea-floor spreading in the Woodlark basin. *Nature*, **374**, 534–537.

TRON, V. & BRUN, J.-P. 1991. Experiments on oblique rifting in brittle–ductile systems. *Tectonophysics*, **188**, 71–84.

VINK, G.E. 1982. Continental rifting and the implications for plate tectonic reconstructions. *Journal of Geophysical Research*, **87**, 10677–10688.

WATANABE, T., LANGSETH, M.G. & ANDERSON, N.R. 1977. Heat flow in back-arc basins of the Western Pacific. *In*: TALWANI, M. & PITMAN, C.W. (eds) *Island Arcs, Deep Sea Trenches and Back-Arc Basins*. Maurice Ewing Series, American Geophysical Union, **1**, 137–161.

WESSEL, P. & SMITH, W.H.F. 1991. Free software helps map and display data. *EOS Transactions, American Geophysical Union*, 441, **72**, 445–446.

WHITMARSH, R.B. & MILES, P.R. 1995. Models of the development of the West Iberia rifted continental margin at 40°30′N deduced from surface and deep-tow magnetic anomalies. *Journal of Geophysical Research*, **100**, 3789–3806.